NIPPON STEEL TECHNICAL REPORT No. 122 NOVEMBER 2019

Technical Report

UDC 629 . 11 . 011 : 669 . 14 . 018 . 26

Research on Axial Collapse Structures Applying Advanced High-strength Steel Sheet

Yutaka MIKAZUKI* Yoshiaki NAKAZAWA
Masahiro NAKATA

Abstract

Axial collapse structures in automotive bodies are required for light weight and high energy absorption. In this report, the cross-sectional design and the application of advanced high-strength steel sheets over 980 MPa grade are investigated. It is revealed that a cross-sectional design with a low ratio of width of plane to thickness and the application of thin advanced high-strength steel sheet with excellent bendability are important for attaining light weight and high energy absorption of axial collapse structures.

1. Preface

To reduce vehicle body weight based on reduced vehicle fuel consumption and to ensure collision safety, there is demand for the impact-absorbing members that compose vehicle body frames to be reduced in weight and to have excellent energy absorption performance. Some impact-absorbing members absorb energy by plastic deformation arising from continuous buckling in input in the member axial direction (longitudinal direction). This type of member is called an axial collapse structure. The axial collapse structure is arranged at the front and rear of a vehicle, and, in frontal or rear-end collision, it absorbs energy and provides space for occupants.

To improve energy absorption of the axial collapse structure, effective measures are control of load characteristics and buckling deformation behavior by cross-sectional design as well as use of high-strength materials. Many studies on cross-sectional design have been conducted, and buckling deformation behavior characteristics of square tube members[1)] and control of buckling deformation behavior[2)] have been reported. High-strength materials, on the other hand, should not cause discontinuous deformation progress by fracture in axial collapse in addition to ensuring stable buckling deformation behavior, and steel with a strength of 590 to 780 MPa grades is mainly used at present.

This paper discusses the cross-sectional design and application of steel over 980 MPa grade for developing an axial collapse structure with light weight and excellent energy absorption performance. Chapter 2 first describes investigation of cross-sectional shape factors for improving the energy absorption performance by using a 590 MPa grade polygonal member. Chapter 3 describes the effects of the material strength on buckling deformation behavior and the review result of deformation in the material fracture area. Chapter 4 provides a description of performing cross-sectional design of an axial collapse structure using a 1180 MPa grade material based on the findings in Chapter 2 and Chapter 3, and reports the test results of the weight reduction feature and the energy absorption performance.

2. Cross-sectional Shape Factor for Improving Energy Absorption Performance

To study the energy absorption performance in axial collapse and effects of cross-sectional shapes on buckling deformation behavior, details of numerical analysis under conditions of various cross-sectional sizes and thicknesses of tetragonal, hexagonal, and octagonal shapes are described.[3, 4)]

2.1 Analysis conditions

In numerical analysis, a dynamic explicit FEM was used. **Figure 1** shows a schematic view of the FEM model. First, to review the effects of width of plane W_p, analysis was conducted for the cases of circumradius R = 30, 60, and 120 mm and number of ridge lines N_r = 4, 6, and 8 (W_p = 21.5 to 153.7 mm). Thickness t was 1.6 mm for all materials. Then, for the effect of thickness t, analysis was performed for the cases of thickness t = 1.0, 1.6, and 2.0 mm where circumradius R = 60 and number of ridge lines N_r = 8 were fixed. In addition, to investigate the mutual effect between width of plane W_p and thickness t, analysis was performed for R = 30, 60, and 120 mm (W_p = 21.5 to 153.7 mm), number of ridge lines N_r = 4, 6 and 8, and thickness t = 1.0, 1.6, and 2.0 mm. For each model, curvature radius

* Researcher, Integrated Steel-Solution Research Lab., Steel Research Laboratories
20-1 Shintomi, Futtsu City, Chiba Pref. 293-8511

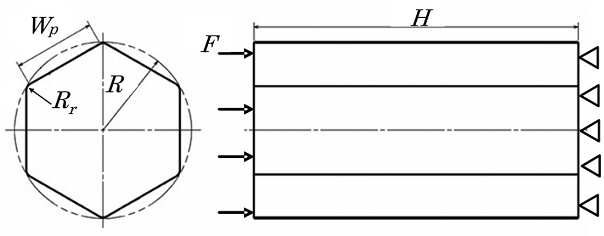

Fig. 1 FEM model of thin-walled polygonal shell member (N_r=6)

R_r at the ridge section was 4 mm and member length H was 220 mm.

A rigid wall was collided with in the member axial direction at speed V = 15 km/h (4.17 m/s). Also, the collision side end was restrained except for the case of translational motion in the member axial direction, and the opposite collision side end was completely restrained.

The sample member was a BWC shell element with a mesh size of about 2 mm square. Assuming 590 MPa grade material for the member, the result obtained from the tensile test was subjected to poly-linear approximation analysis for the relationship between the equivalent stress and equivalent plastic strain. The Cowper-Symonds law was applied to the strain rate dependency.

2.2 Effect of width of plane W_p

First, the effect of width of plane W_p on displacement and load is described. **Figure 2** shows a displacement vs. load diagram with circumradius R = 30, 60, and 120 mm and number of ridge lines N_r = 8. The horizontal axis in the figure is displacement δ of the rigid wall and the vertical axis is load F/L per circumferential length obtained by dividing load F by circumference L of the member cross section. The red solid line, blue broken line, and black solid line are circumradius R = 30, 60, and 120 mm, respectively, and correspond to width of plane W_p = 21.5, 43.0, and 86.0 mm. Attention is paid to the case of R = 30 and N_r = 8. It can be seen that the load repeatedly increases and decreases along with the increase in displacement δ. This interval of increase/decrease corresponds to the buckling wavelength in which one buckling wrinkle is generated and folded in axial collapse. It can be seen that the buckling wavelength becomes larger along with the increase in width of plane W_p. In contrast, the maximum point of load is found to become smaller along with the increase in width of plane W_p.

Next, the effect of width of plane W_p on the energy absorption performance and buckling wavelength D_b is described. In **Fig. 3**, average load F_{ave}/L per circumferential length of each circumradius R of 30, 60, and 120 mm and each of the numbers of ridge lines N_r of 4, 6, and 8, and buckling wavelength D_b are plotted. A high average load means high energy absorption performance. The horizontal axis in the figure is width of plane W_p, and the vertical axis is average load F_{ave}/L per circumferential length and buckling wavelength D_b. Similar to the result of N_r = 8 in Fig. 2, if width of plane W_p is shortened, it was found that a deformed shape with a shorter buckling wavelength D_b was obtained, resulting in improved energy absorption performance.

2.3 Effect of thickness t and mutual effect of width of plane W_p and thickness t

First, the effect of thickness t on the displacement and load is described. **Figure 4** shows a displacement vs. load diagram with circumradius R = 60 mm, number of ridge lines N_r = 8 (W_p = 43.0 mm), and thickness t = 1.0, 1.6, and 2.0 mm. The horizontal axis in the figure is displacement δ of the rigid wall, and the vertical axis is

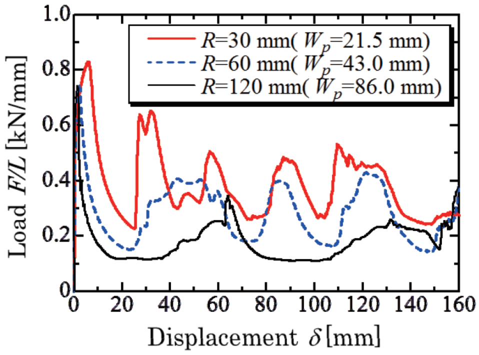

Fig. 2 Effect of the width of plane W_p, on load-displacement responses (N_r=8)

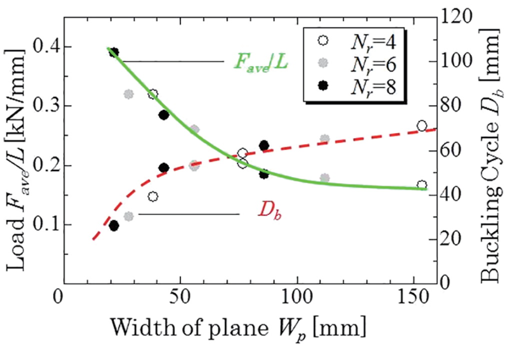

Fig. 3 Effect of the width of plane W_p, on the average load F_{ave}/L, and the buckling cycle D_b

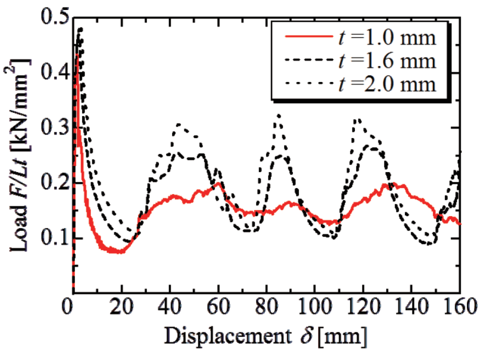

Fig. 4 Comparison of load-displacement responses with respected to the thickness t (N_r=8, R=60)

load F/Lt per cross-sectional area obtained by dividing load F by area Lt of the member cross section. With thickness t = 1.6 and 2.0 mm, the maximum point is clear even after the first maximum point of load. In contrast, with thickness t = 1.0 mm, the maximum point is not clear after the first maximum point of load and load fluctuation is small. Although the cross section is standardized, load F/Lt at the maximum point varies depending on thickness t. Therefore, the load history in axial collapse is found to depend on thickness t in addition to width of plane W_p.

Next, the mutual effect of width of plane W_p and thickness t on the energy absorption performance is described. **Figure 5** shows the relationship between average load F_{ave}/Lt per cross-sectional area and thickness ratio of width of plane W_p/t. This indicates that aver-

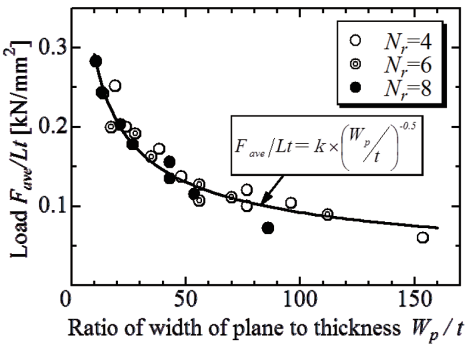

Fig. 5 Relationship between the thickness ratio of width of plane W_p/t, and average load F_{ave}/Lt (N_r=4, 6, 8)

age load F_{ave}/Lt is represented by the single curve with the parameter of thickness ratio of width of plane W_p/t. The lower the thickness ratio of width of plane W_p/t is, the higher the average load F_{ave}/Lt is. In this way, the energy absorption efficiency is improved. This proves that a cross-sectional shape with a small W_p/t, which improves the energy absorption performance, should be the target in cross-sectional design.

3. Study for Application of Advanced High-strength Steel for Axial Collapse Members

Described below are the results of studies on buckling deformation behavior of materials with high yield stress and fracture behavior of the materials as problems when advanced high-strength steel sheet is applied to axial collapse members.

For buckling deformation behavior, it is known that, if the ratio of the thickness to the one-side length of a square tube cross section, and if the square cross section is smaller than 2%, non-compact mode without folding at equal intervals may occur.[1] The thickness ratio of width of plane W_p/t described in Chapter 2 is one of the geometrical factors governing bending rigidity in the plane region,[4] and the same applies to the ratio of the thickness to the side length. Therefore, changes in buckling deformation behavior are related to deflection, in other words, out-of-plane deformation, in the plane region. When the out-of-plane deformation is large, non-compact mode may occur. In this chapter, focus is placed on out-of-plane deformation in the plane region, and the material strength and the effect of the cross section on buckling deformation behavior are studied using numerical analysis.

For the fracture behavior of the material, the progress of cracks in the axial direction as shown in **Fig. 6** is serious since this may result in discontinuation of buckling deformation progress. In this paper, this fracture is called longitudinal fracture. In this chapter, strain at the longitudinal fracture in Fig. 6 is observed using numerical analysis, and the deformation state at the fracture and the effect of the cross-sectional shape and thickness on risk of fracture are studied.

3.1 Analysis conditions

Dynamic explicit FEM was used for the numerical analysis. The sample member was determined to be a regular square tube member (hereinafter simply referred to as a square tube member). Analysis was performed for the cases with a thickness of t = 1.6 mm and a cross-sectional outline dimension of W = 40 and 60 mm (W_p/t = 19 and 31) and with a thickness of t = 1.0 mm and a cross-sectional outline dimension of W = 29 mm (W_p/t = 19). The materials used were two levels of 590 and 980 MPa grades. For both cases, curvature radius R_r at the ridge line was 5 mm and member length H was 250 mm. A list of the analysis conditions is shown in **Table 1**.

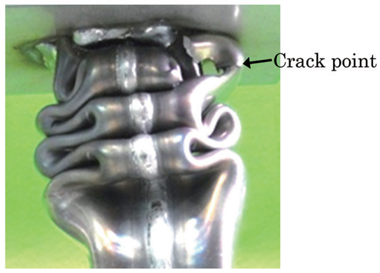

Fig. 6 Example of crack during axial collapse deformation

Table 1 Materials and dimensions

Material		Cross-sectional outer dimension W [mm]	W_p/t
Thickness t [mm]	Grade		
1.6	590 MPa	60	31
1.6	980 MPa	60	31
1.6	980 MPa	40	19
1.0	980 MPa	29	19

A rigid wall was collided with in the member axial direction at speed V = 27.6 km/h (7.6 m/s). Also, the collision side end was restrained to the rigid body and the opposite collision side end was completely restrained.

The sample member was the BWC shell element and the mesh size was about 2 mm square. For the material characteristics of the 590 and 980 MPa grades, the result obtained from the tensile test was subjected to poly-linear approximation analysis for the relationship between the equivalent stress and equivalent plastic strain. The Cowper-Symonds law was applied to the strain rate dependency.

3.2 Effect of material strength and cross-sectional shape on buckling deformation behavior

Focus was placed on the out-of-plane deformation in the plane region of the square tube member. The effect of the material strength and cross section on the buckling deformation behavior was investigated. In **Fig. 7**, the out-of-plane deformation at the plane region center is calculated along the member axial direction from the collision side and plotted. The horizontal axis in the figure is coordinate Z in the member axial direction and the vertical axis is out-of-plane deformation δ_p. Position 0 in the horizontal axis corresponds to the end on the collision side. This figure indicates the result of displacement δ = 2.5 mm equivalent to the value immediately after occurrence of initial buckling. At all levels, the out-of-plane deformation is large at the collision side end and this corresponds to the area where buckling wrinkles are formed.

First, the effect of the material strength on the out-of-plane behavior is described. Figure 7 (a) shows the results of 590 MPa grade and 980 MPa grade for W_p/t = 31 and t = 1.6 mm. Compared with the 590 MPa grade, the 980 MPa grade has large out-of-plane deformation. Since advanced high-strength steel sheet has high yield stress, this could be caused by increasing the out-of-plane deformation in terms of elasticity before plastic buckling. As a result of detailed comparison, in the 980 MPa grade, out-of-plane deformation is found in the area where buckling wrinkles larger than 100 mm for coordinate Z in the member axial direction do not form. As de-

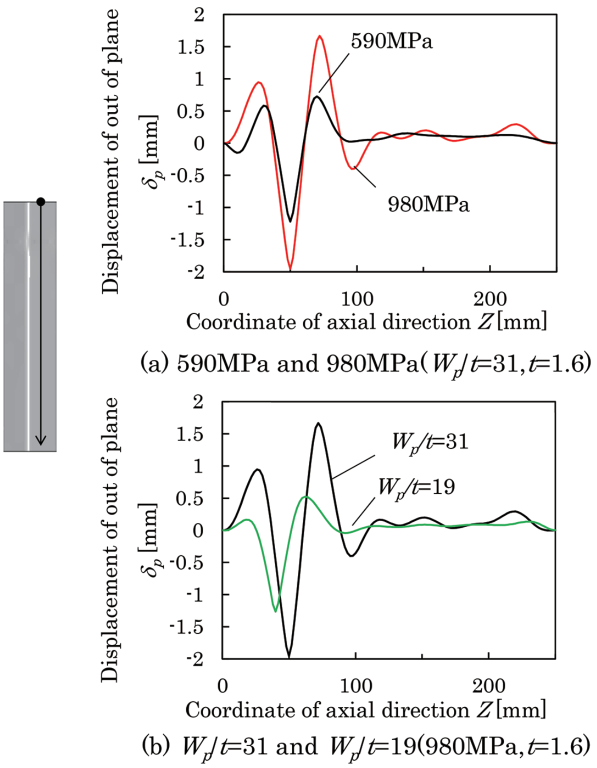

Fig. 7 Comparison of displacement of out-of-plane at the plane of square tube members

scribed above, use of advanced high-strength steel sheet increases out-of-plane deformation in the plane region, suggesting a high possibility of occurrence of non-cyclic non-compact mode, namely, unstable progress of deformation.

Next, the effect of the cross-sectional shape on the out-of-place deformation behavior is described. Figure 7 (b) shows the results of the 980 MPa grade with W_p/t = 19 and W_p/t = 31, in t = 1.6 mm. Compared with W_p/t = 31, W_p/t = 19 has smaller out-of-plane deformation, and the out-of-plane deformation in the area where buckling wrinkles do not form is small. Therefore, as one measure for suppressing the progress of unstable buckling, it is considered that a small W_p/t and high bending rigidity in the plane region are effective for high strength.

3.3 Deformation status at fracture

The strain states, such as the distribution in the thickness direction by the difference in shell front/back of the maximum principal strain in numerical analysis and the direction of maximum principal strain, are observed, and clarification of the deformation state at the fracture is attempted. Two sides facing each other in the cross section of the square tube member cause outward out-of-plane deformation due to buckling, and the remaining two sides cause inward out-of-plane deformation. From Fig. 6, it is estimated that longitudinal fracture has occurred near the end of the sides deformed inward. The area is called a fracture area here and attention should be paid to the strain state of the fracture area.

Figure 8 shows a contour diagram of the maximum principal strain for the steel with W_p/t = 19, 980 MPa grade, and t = 1.6 mm. Figure 8 (a) shows the maximum principal strain at the integration point nearest the surface layer inside the square tube member and Fig. 8 (b) shows the maximum principal strain at the integration point nearest the surface layer outside the square tube member. The

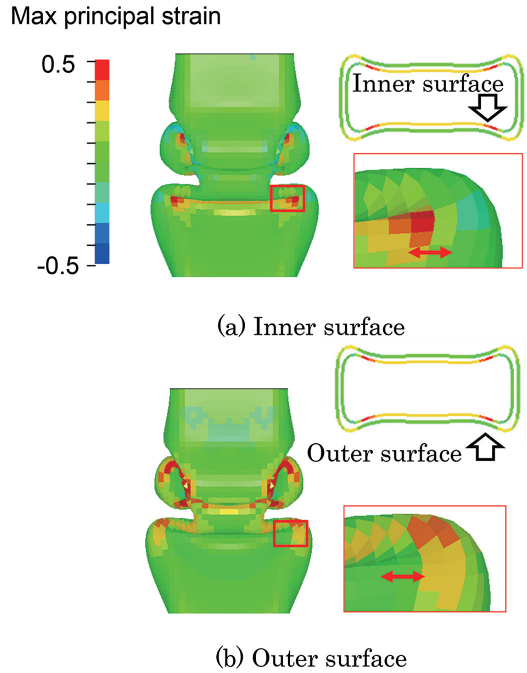

Fig. 8 Deformation at the crack point (W_p/t=19, 980 MPa, t=1.6 mm)

figure on the upper right of each figure is a cross section. The red frame indicates the enlarged cross section. The maximum principal strain inside the square tube member in Fig. 8 (a) is large tensile strain and the direction thereof is orthogonal to the axial direction of the square tube member. The value of the maximum principal strain exceeds 0.4 at the maximum point. In contrast, the maximum principal strain outside the square tube member in Fig. 8 (b) is strain similar to that due to compression and the direction thereof is orthogonal to the axial direction of the square tube member. From the above, it was found that strain in the fracture area is directed inward and is tensile strain, and that a strain gradient was observed in the thickness direction. From these facts, it is estimated that the deformation state in the fracture area is bending deformation with the inside of the square tube member being bent outside.

The bending deformation has a strain gradient in the thickness direction and the deformed state is different from that in the tensile test, which causes uniform strain in the thickness direction. To this end, for the fracture limit (bending property) in bending deformation, study using 90° V-block bending or tensile bending has been reported.[5–7] Also, a high fracture limit strain of the surface layer for 90° V-block bending has been reported in comparison with elongation of the tensile test.[5] Structural factors for material bendability have been reported.[8] As described above, it is suggested that bendability of the material is important in suppressing fracture under bending deformation.

3.4 Effect of cross-sectional shape and thickness on risk of fracture

Section 3.3 described the fracture area being the bending deformation state. Here, the maximum principal strain values of the numerical analysis are compared and the effect of the cross-sectional shape and thickness on risk of fracture is described. **Figure 9** shows a contour diagram of the maximum principal strain at the integration point nearest the surface layer inside the square tube member. Figure 9 (a) shows the results of the 980 MPa grade with W_p/t = 31 and

t = 1.6 mm, Fig. 9 (b) shows the results of the 980 MPa grade with W_p/t = 19 and t = 1.6 mm, and Fig. 9 (c) shows the results of the 980 MPa grade with W_p/t = 31 and t = 1.0 mm. In all figures, the red framed area corresponding to the fracture area is enlarged. Since the largest strain area may have high risk of fracture, attention is paid to the strain level of the area. The strain outside the square tube member at the highest strain area is similar to that due to compression. It can be found that the deformation state in the area is the bending deformation state.

To describe the effect of W_p/t, the strain levels of the 980 MPa grade with W_p/t = 31 and t = 1.6 mm in Fig. 9 (a) and the 980 MPa grade with W_p/t = 19 and t = 1.6 mm in Fig. 9 (b) are compared. Although Fig. 9 (a) and Fig. 9 (b) have the same thickness, the strain differ depending on the difference in W_p/t, showing a higher strain at a smaller W_p/t level. From this, the cross section with a small W_p/t increases the energy absorption efficiency and this suggests increased fracture risk. This trend conforms to the research result[9] using the octagonal cross section.

Next, the strain level of the 980 MPa grade with W_p/t = 19 and t = 1.6 mm in Fig. 9 (b) and the strain level of the 980 MPa grade with W_p/t = 19 and t = 1.0 mm in Fig. 9 (c) are compared, and the effect of thickness t is described. Figure 9 (b) and Fig. 9 (c) have the same W_p/t, but the strain vary depending on the difference in thickness, indicating a lower level with a smaller thickness. The surface layer strain in bending deformation is represented by ratio R/t of bending curvature radius R and thickness t. The larger this value is, the lower the strain of the bending layer is. In the case of the same curvature radius R, R/t of t = 1.0 is large compared with the case of t = 1.6. In contrast, curvature radius R at the buckling area is considered to be small when it is folded small with a short buckling wavelength. As described in Chapter 2, the buckling wavelength is small with a smaller cross section of width of plane W_p, in other words, 980 MPa grade with W_p/t = 19 and t = 1.0 mm. However, in comparison with the effect of curvature radius R on the strain of the surface layer, it is considered that the effect of thickness is dominant. From the above, thinning of the thickness may reduce the strain of the surface layer in axial collapse and may be effective for suppression of fracture.

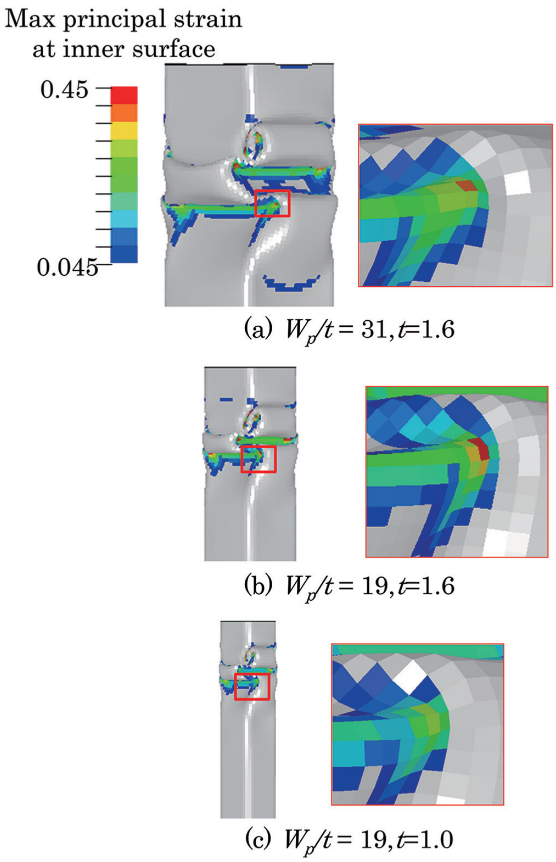

Fig. 9 Comparison of strain at inner surface between 980 MPa results

4. Verification of Reduction of Weight by Cross-sectional Design and High Strength and of the Effect on Energy Absorption Performance

It has been described that it is effective, from the above studies, to use a small cross section of W_p/t with a short buckling wavelength to improve the energy absorption performance and to suppress the progress of unstable buckling in using advanced high-strength steel sheet, and also that it is important to have material bendability and thinning for reduction of bending strain in order to suppress longitudinal fracture in using advanced high-strength steel sheet. Based on these studies, the cross section of the axial collapse member was designed when advanced high-strength steel sheet was used. In addition, we constructed such an axial collapse member and verified reduction of weight and the effect on the energy absorption performance.

4.1 Test conditions

The external dimensions of the member cross section were determined to be 80×80 mm, and the test was performed for the members at two levels shown in **Fig. 10** and **Table 2**.

The cross-sectional shape of Member 1 was a square tube shape (Shape I) shown in Fig. 10 (a) and the material of Member 1 was 590 MPa grade with a thickness of 1.8 mm. In contrast, Member 2 maintained the external dimensions with a small width of plane W_p. Considering improvement of the energy absorption performance and suppression of unstable buckling deformation behavior in using advanced high-strength steel sheet, a cross-sectional shape was de-

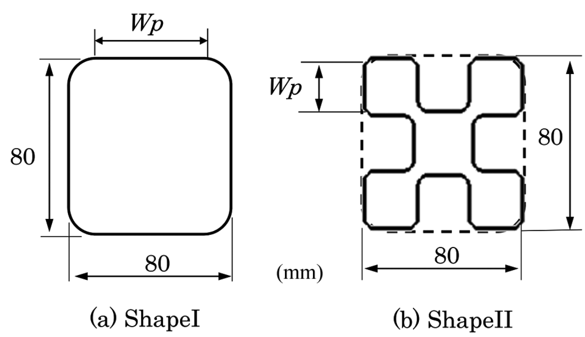

Fig. 10 Cross-sectional shape

Table 2 Conditions of two structures

Structure	Shape	Material: Thickness t [mm]	Material: Grade	W_p/t	Mass [kg]
1	I	1.8	590 MPa	39	1.12
2	II	0.8	1180 MPa	20	0.77

signed. Member 2 had a polygonal cross-sectional shape (Shape II) by providing concave areas at the center of the four sides of the square tube member shown in Fig. 10 (b). For the thickness of the Member 2 material, a material of 0.8 mm was adopted considering reduction of bending strain in buckling deformation due to thinning. In addition, the material for Member 2 used had a strength of 1180 MPa grade and excellent bendability. Member 1 had a W_p/t of 39 and Member 2 had a W_p/t of 20. Both of the member lengths H were 250 mm. In comparison with Member 1, Member 2 was lighter in weight by 30% or more.

A flat-plate impactor was collided with in the member axial direction at speed V = 36 km/h (10 m/s) against Member 1 and Member 2. At both the collision end and the opposite collision end, the end plates with a thickness of 9 mm were welded to the members and the opposite collision side ends were fixed with bolts.

4.2 Test results

First, the deformation states of Member 1 and Member 2 are described. **Figure 11** shows the appearance of the members after the test. Member 2 with a small W_p is deformed in a short buckling wavelength compared with Member 1 and a large number of buckling wrinkles can be seen. No longitudinal fracture can be found on both Member 1 of 590 MPa grade and Member 2 of 1180 MPa grade.

Next, the energy absorption performances of Member 1 and Member 2 are described. **Figure 12** shows a displacement vs. load diagram. The horizontal axis in the figure is displacement δ of the impactor and the vertical axis is load F. Member 2 maintains a higher load value than that of Member 1, and the load increases and decreases at small intervals. The average load of Member 2 is higher by about 1.6 times than that of Member 1.

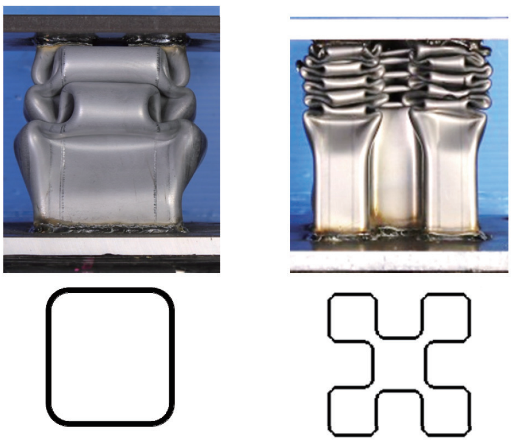

(a) Structure1 (b) Structure2

Fig. 11 Comparison of deformation after crash tests

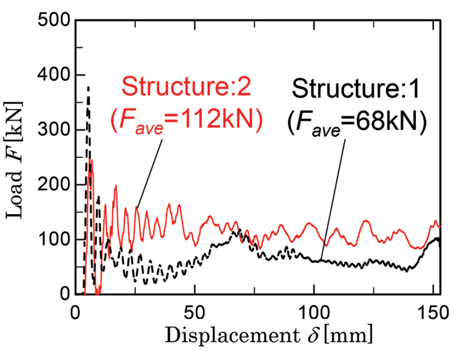

Fig. 12 Comparison of displacement-load

The tests above have verified that the energy absorption performance can be increased and that the weight can be reduced by applying 1180 MPa grade steel sheet, which is thin and excellent in bendability, to the member with a cross-sectional shape designed with a small W_p/t. In comparison with the 590 MPa grade square tube member, the effect is that the energy absorption performance was increased by about 1.6 times and that the weight was reduced by 30% or more.

5. Conclusion

In this paper, use of the cross-sectional design and steel sheet over 980 MPa grade was investigated to reduce the weight of the axial collapse member and to achieve high energy absorption performance, and we have found that the following elements are important.

(1) The energy absorption performance of the axial collapse member can be increased by reducing thickness ratio of width of plane W_p/t of the member cross section.
(2) Use of advanced high-strength steel sheet increases out-of-plane deformation in the plane region of the member, which suggests that progress of unstable buckling is induced. It is important to increase bending rigidity of the plane region by reducing W_p/t to suppress the progress of unstable buckling.
(3) It has been suggested that the deformation state of the fracture area in axial collapse is attributable to bending deformation. To suppress fracture, it is important to reduce the material thickness, decrease the bending strain, and maintain bendability of the material.

Considering these elements, the cross section and thickness were designed and 1180 MPa grade steel sheet excellent in bendability was used. In result, in comparison with the 590 MPa grade square tube member, the tests have proved weight reduction by 30% or more and improved energy absorption performance by about 1.6 times.

In the future, we will conduct further studies to use the elements described in this paper for the axial collapse members of actual vehicle bodies.

References

1) Mahmood, H.F. et al.: Trans. SAE. 90, Section 4, 4039–4050, (1981), Paper No.811302
2) Hirose, S. et al.: The Proceedings of the 62nd Japanese Joint Conference for the Technology of Plasticity. 62, 563–564 (2011)
3) Nakazawa, Y. et al.: Transactions of the JSME (in Japanese), Edition A. 73 (727), 331–337 (2007)
4) Nakazawa, Y. et al.: Transactions of the JSME (in Japanese), Edition A. 73 (731), 828–834 (2007)
5) Yonebayashi, T. et al.: The Proceedings of the 2011 Japanese Spring Conference for the Technology of Plasticity, 2011, p.273–274
6) Shirakami, S. et al.: The Proceedings of the 2012 Japanese Spring Conference for the Technology of Plasticity, 2012, p.7–8
7) Yonebayashi, T. et al.: The Proceedings of the 62nd Japanese Joint Conference for the Technology of Plasticity. 62, 367–368 (2011)
8) Yamazaki, K. et al.: Journal of the Japan Society for Technology of Plasticity. 36 (416), 973–978 (1995)
9) Tanaka, Y. et al.: Transactions of the JSME (in Japanese), Edition A. 78 (791), 955–965 (2012)

Yutaka MIKAZUKI
Researcher
Integrated Steel-Solution Research Lab.
Steel Research Laboratories
20-1 Shintomi, Futtsu City, Chiba Pref. 293-8511

Masahiro NAKATA
Chief Researcher
Integrated Steel-Solution Research Lab.
Steel Research Laboratories

Yoshiaki NAKAZAWA
General Manager, Head of Dept., Dr.Eng.
Research Administration Dept.
R & D Planning Div.